




STS observations of deep defects within laser-illuminated graphene/MOVPE-h-BN heterostructures

Cite as: Appl. Phys. Lett. **114**, 102103 (2019); <https://doi.org/10.1063/1.5081487>

Submitted: 15 November 2018 . Accepted: 26 February 2019 . Published Online: 13 March 2019

I. Wlasny , K. Pakula, R. Stepniewski, W. Strupinski, I. Pasternak , J. M. Baranowski, and A. Wyszomlek 



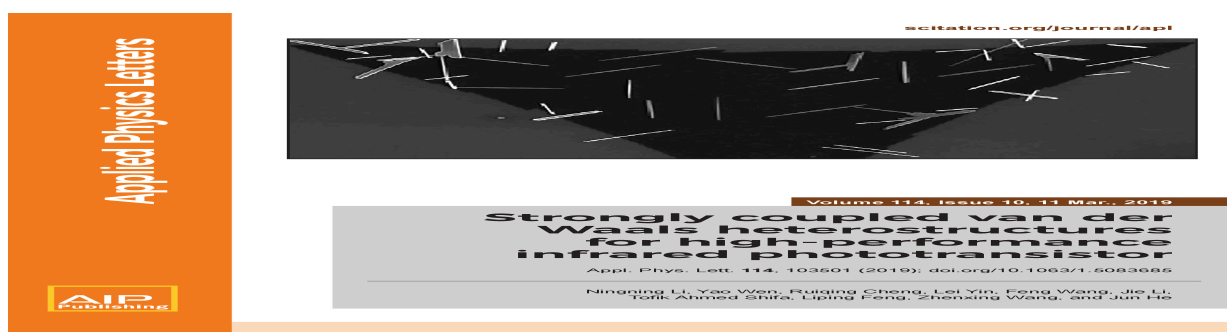
View Online



Export Citation



CrossMark



STS observations of deep defects within laser-illuminated graphene/MOVPE-h-BN heterostructures

Cite as: Appl. Phys. Lett. **114**, 102103 (2019); doi: [10.1063/1.5081487](https://doi.org/10.1063/1.5081487)

Submitted: 15 November 2018 · Accepted: 26 February 2019 ·

Published Online: 13 March 2019



View Online



Export Citation



CrossMark

I. Wlasny,^{1,a)}  K. Pakula,¹ R. Stepniewski,¹ W. Strupinski,² I. Pasternak,²  J. M. Baranowski,³ and A. Wyszomlek¹ 

AFFILIATIONS

¹Institute of Experimental Physics, Faculty of Physics, University of Warsaw, Pasteura 5, 02-093 Warsaw, Poland

²Faculty of Physics, Warsaw University of Technology (WUT), Koszykowa 75, 00-662 Warsaw, Poland

³Institute of Electronic Materials Technology, Wolczynska 133, 01-919 Warsaw, Poland

^{a)}Electronic mail: igor.wlasny@fuw.edu.pl

ABSTRACT

We present the study of metalorganic vapor phase epitaxy hexagonal boron nitride (MOVPE-h-BN) and graphene/MOVPE-h-BN heterostructures under the illumination with monochromatic light. The process of illumination makes the modification visible by both the shifting of Raman lines and the emergence of local electric fields. These changes are related to the modification of the charge state of the deep defect centers and can be used to control other 2D materials within heterostructures. The scanning tunneling spectroscopy study of the graphene/MOVPE-h-BN heterostructure allowed us to observe the defect states associated with the h-BN and evaluate the effect of illumination on them as well as the electronic structure of graphene.

Published under license by AIP Publishing. <https://doi.org/10.1063/1.5081487>

Two-dimensional materials attract growing attention of the scientific community due to the wide range of exceptional properties,^{1,2} the most important of which include their atomic thickness, offering potential downsizing of the technology. Because of their unique traits, they are considered for various applications in biosensors,³ biomedicine,⁴ flexible nanoelectronics,^{2,5} or photovoltaics.⁶

One of the most widely researched 2D materials is hexagonal boron nitride (h-BN)—a semiconductor with a wide, over 5.9 eV, bandgap.⁷ What is more, its surface is exceptionally flat, which prevents spatial inhomogeneities in surface static charge,^{8,9} the problem of which exists in currently used substrates, such as SiO₂.¹⁰ This makes it an excellent material for insulating applications.

For 2D materials, particularly important is the possibility of creating layered vertical heterostructures, where a broad range of properties of the system can be tailored and adjusted.^{11,12} The heterostructure composed of the aforementioned materials—graphene and h-BN, is proposed for various applications, such as photovoltaics^{6,13} or electronics,¹⁴ where encapsulating graphene in h-BN leads to an increase in charge carrier mobility.⁹

The above described properties of the two-dimensional nanomaterials, graphene and h-BN in particular, give promise of creating complex electronic and optoelectronic systems, while maintaining a small

size required by trends of miniaturization of technology. This is particularly true given the possibility of tailoring the properties of these structures, either during or post growth. Particularly interesting synthesis methods involve simple, easily controlled processes. Recent reports show that the illumination of either single- or multi-layers of this material leads to the emergence of local electric fields.^{15,16} This effect may be used to control the strain and charge carrier density in graphene within a single heterostructure,¹⁵ providing means for simple and reversible¹⁶ tailoring of the properties of a heterostructure.

The focus of this study is on hexagonal boron nitride synthesized using the metalorganic vapor phase epitaxy (MOVPE) method. It is motivated by the fact that even though such a material may have higher defect density, it allows for large-area synthesis and, therefore, has much higher applicational value.

The MOVPE method allowed us to synthesize the h-BN material with prevalent sp² in-plane bondings—the stacking is not considered. Layers were produced using the following process. Ammonia (NH₃) and triethylboron (TEB) were used as precursors and hydrogen (H₂) as a carrier gas. Growth of the h-BN layers for the samples used in the experiment was performed in the pulsed mode, giving a continuous, 18 nm thick layer, with hexagonal symmetry axis perpendicular to the substrate surface.

The topography of a surface of the sample after the boron nitride deposition, as measured by atomic force microscopy (AFM), is shown in Fig. 1(a). Upon inspection, a number of steps or terraces can be seen. Their width is estimated to be $1.0 \pm 0.5 \mu\text{m}$ and height to be about $2 \pm 1 \text{ nm}$. These values are in agreement with acceptable misorientation of the crystallographic alignment of the used substrate surface and thus are assumed to be surfaces of the well-defined h-BN material. Furthermore, additional features can be found in the form of long, thin, anisotropically arranged areas. They are found to be $8 \pm 2 \text{ nm}$ thick. They are most likely morphological defects, where the layer grows perpendicularly to the surface, created during the growth of the material.

With a purpose of fabricating the heterostructure by chemical vapor deposition (CVD), graphene has been used. The material has been grown on copper foil as a single layer.¹⁷ In order to transfer the graphene layer onto the h-BN, it has been coated with a polydimethylsiloxane (PDMS) layer. Copper has been etched with 0.1 M solution of ammonium persulfate $[(\text{NH}_4)_2\text{S}_2\text{O}_8]$.¹⁸ After the deposition of graphene, the PDMS film has been removed during the cooling phase after previously heating the sample up to 90°C .¹⁹ In order to enable STM/scanning tunneling spectroscopy (STS) measurements, electric contacts have been created on the graphene surface using an isopropanol-based silver colloid. The topography after the graphene deposition is shown in Fig. 1(b). After the deposition, roughness of the

surface has increased. What is more, wrinkle-like structures have appeared. They were most likely created during the heating of the PDMS with graphene layers, as the thermal expansion coefficients of these two materials are different.¹⁹ It is interesting that in STM topographies, as shown in Fig. 1(d), a network of lines is found, which are likely associated with the wrinkles of the h-BN material, which have appeared due to the negative thermal expansion coefficient of boron nitride.²⁰ The presence of transferred graphene was confirmed by the scanning tunneling microscopy measurements, where the presence of conductive layers enables the experiment. What is more, topographies performed with sub-nanometer resolution on atomically flat terraces [see Fig. 1(c)] reveal a honeycomb structure of the material. No moire pattern is observed, indicating no high-symmetry alignment of h-BN and graphene layers.²¹ There is a visible variation of the structure, however, showing a degree of interaction between graphene and h-BN electronic structures.

The Raman spectroscopy (RS) measurements performed on the sample confirm the presence of hexagonal boron nitride layers, with the line located at 1366 cm^{-1} and full width at half maximum (FWHM) of 22 cm^{-1} [Fig. 1(e)]. While the width of the line is significantly higher than that of the single crystal or exfoliated layers,¹⁵ it does correspond to a high quality MOVPE material.²² The line energy is also slightly higher compared to that of exfoliated flakes.^{15,23} This suggests that the material is subjected to a slight mechanical strain. This fact is most likely related to the strain induced during the post-growth cooling. What is more, a significant luminescence is observed. This effect is related to the presence of various deep defect states, including single photon emitters, in the structure of h-BN.²⁴ It is worth noting that, as seen in Fig. 1(e), the intensity of the luminescence decreases during the illumination of the sample, thus suggesting that the state of the centers is changed in the process.

In addition to the initial characterization of the boron nitride, Raman spectroscopy has also been used to investigate the effect of illumination on the layers. As an excitation source, a 532 nm laser has been used. The beam has been focused on the sample with $100\times$ objective providing a $0.25 \mu\text{m}^2$ circular spot. Since the previous reports¹⁵ indicate that the results are similar for a wide range of power densities, a set of optical filters has been used, which resulted in 1.3 mW of power being provided onto the illuminated area. This value allows, in the presented case, to balance the stability of the experimental conditions, while providing the best temporal resolution of the measurements.

During the process, the Raman shift of the E_{2g} line moves towards higher values for about 1 h, as seen in Fig. 2(c). Afterwards, the line energy decreases and reaches a stable level. The E_{2g} line position of the hexagonal boron nitride is related to the strain of the crystal lattice of the material.²⁵ The strain is a result of the interaction between the charged localized deep defect centers of h-BN. These changes are directly caused by the photoionization of the deep defect centers by light. The observed behavior is similar to that reported for the exfoliated material.¹⁵ This fact suggests that the distribution of the defects is similar in both cases.

The illumination experiment is performed *in-situ*, during RS measurements, on graphene/h-BN heterostructures in order to provide information on the evolution of the G and 2D band positions. Based on the data, the Gruneisen model has been used in order to estimate the changes in the electron concentration within the

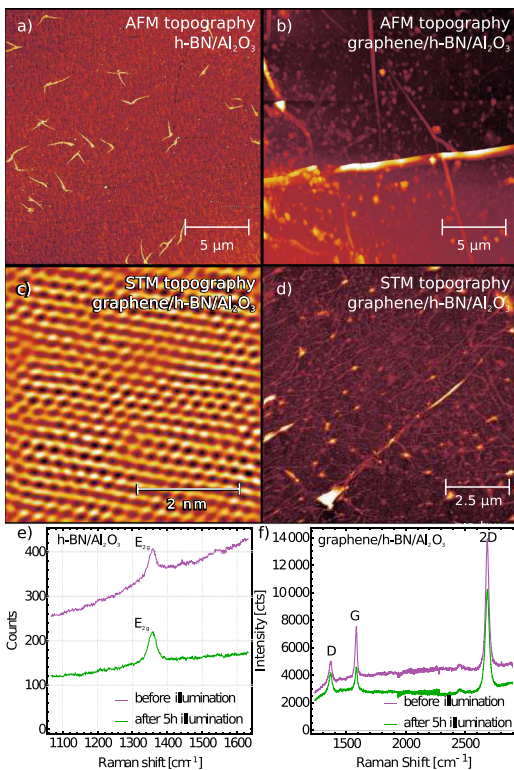


FIG. 1. AFM topography images of the h-BN sample (a) before and (b) after graphene deposition. STM image of the graphene/h-BN (c) on a sub-micron scale with atomic resolution and (d) on a micro-scale; Raman spectra of the (e) h-BN sample and (f) G/h-BN heterostructure before and after the illumination.

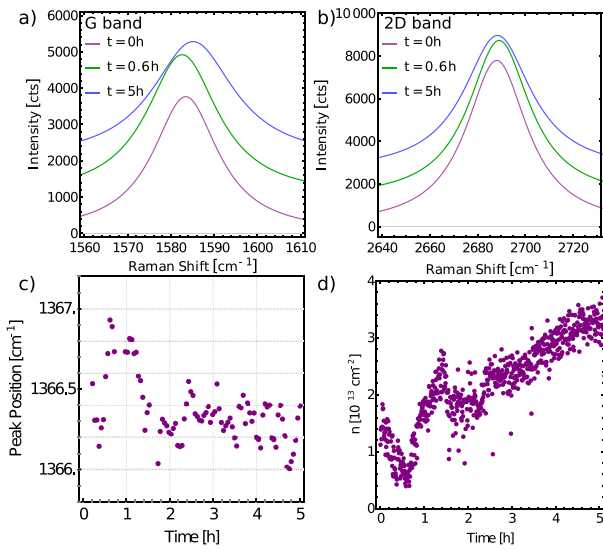


FIG. 2. (a) G and (b) 2D bands of graphene within the G/h-BN heterostructure before and during illumination, (c) changes of the E_{2g} h-BN Raman line during illumination of the as-grown material with a 532 nm 1.3 mW laser over $0.25 \mu\text{m}^2$, each experimental point was taken after 180 s, and (d) changes of the electron density in the h-BN/graphene heterostructure during illumination with a 532 nm 1.3 mW laser over $0.25 \mu\text{m}^2$ and 30 s temporal resolution.

graphene^{26,27} with an assumption of the low n-type doping of graphene and the presence of biaxial strain, the plot of which is shown in Fig. 2(d). Initially, the graphene layers exhibit a slight negative doping. For almost an hour of the process, roughly similar time to the increase in the E_{2g} line position, the concentration decreases from about 1.5 to $0.3 \times 10^{13} \text{ cm}^{-2}$. Subsequently, up until 1.5 h into the illumination, the electron concentration increases rapidly. After that time, the rate of the increase is lower and does not seem to change during the remainder of the process.

The observed changes in both h-BN Raman line energy and the electron concentration in graphene within the graphene/h-BN heterostructure are associated with the light-assisted change of the charge state of the defect centers of h-BN.¹⁵ Based on the similar behavior of the investigated MOVPE-based and exfoliated structures,¹⁵ certain similarities between the observations can be found. The initial decrease in the electron concentration [Fig. 2(d)] is associated with the increase in the charge state of the defect centers. During the longer illumination, however, the charge is transported outside the illuminated area.¹⁵ This is correlated with the increase in the electron concentration in graphene, as seen in Fig. 2(d).

In order to provide more information on the involvement of the defect centers in the process, the scanning tunneling spectroscopy (STS) measurements have been performed on both illuminated and non-illuminated graphene/MOVPE-h-BN heterostructures. The illumination process was performed *ex-situ*, using a non-focused 532 nm laser, providing 50 mW monochromatic radiation on the circular spot with a 1 mm radius. The process lasted for 24 h in order to compensate for the lower power density of the non-focused laser beam. After the illumination, the sample was transferred to UHV conditions within 10 min. The experiment was performed using an Omicron GmbH Multiprobe P system working in ultra-high vacuum conditions

(2×10^{-9} Torr) at room temperature. The accumulation was attempted on a $50 \text{ nm} \times 50 \text{ nm}$ area within a 64×64 points grid, lower than in the case of previously shown topographies [Figs. 1(c) and 1(d)], which was necessary in order to retain the stability of the measurement at room temperature. The topography gathered during the STS measurement [Fig. 3(a)] shows terraces or steps of the material, not seen in previous topographies [Figs. 1(c) and 1(d)] due to the difference in scale. dI/dV curves have been gathered in two ranges. The narrow range, spanning between -1 V and $+1 \text{ V}$, was expected to provide information on the Dirac point position, relative to the Fermi level, in graphene. As the previously published reports show that the defect sites of h-BN can be observed using STM,³⁰ the wide range measurement was performed in the range from -3.5 V to $+3.5 \text{ V}$ in order

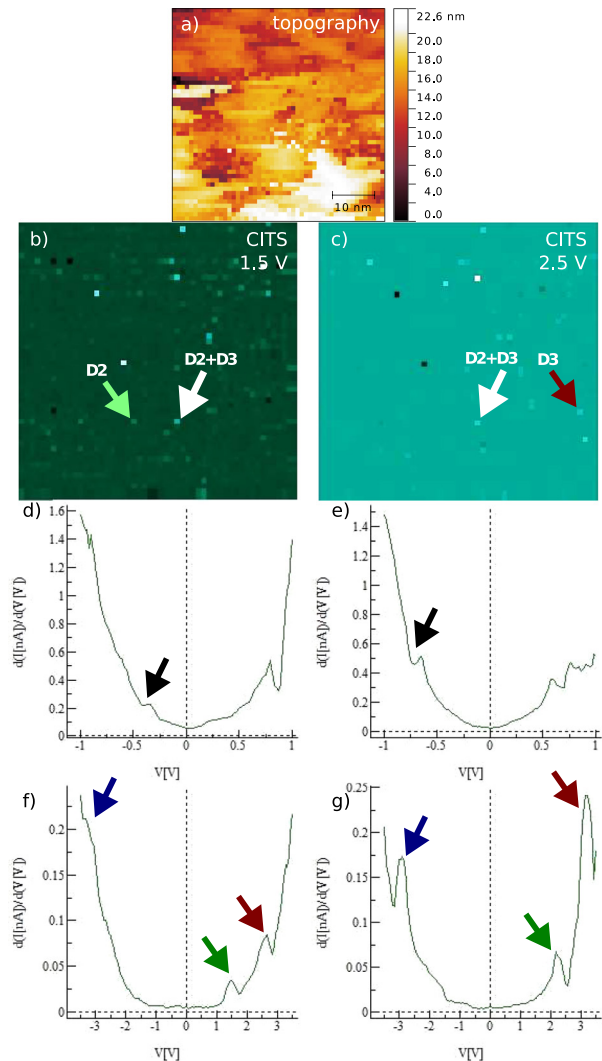


FIG. 3. (a) STM topography of the graphene/h-BN/ Al_2O_3 structure before the illumination taken during the STS measurements, (b) dI/dV map of the area at 1.5 V bias, and (c) dI/dV map of the area at 2.5 V bias. dI/dV curves at the point marked with D2 + D3 arrow in narrow (d) and (e) and wide V range (f) and (g), before (d) and (f) and after the illumination (e) and (g).

to enhance the visibility of h-BN related levels, in particular, those positioned close to the valence and conduction bands. In Fig. 3(d), an exemplary narrow dI/dV curve is shown. At the energy of about -0.35 eV, a dip is seen, which is consistently found in the investigated area. Based on the fact that the dip is seen in the nearly every gathered curve and the fact that the graphene doping type calculated using the Raman spectra prior to illumination is positive (n-type doping), we assume that this is a Dirac point, which is characteristic of the electronic structure of graphene,^{28,29} shifted due to the n-type doping of the material. Several additional maxima are seen at the positive bias. However, their position and count are not consistent within the investigated area and are more likely related to the inhomogeneity of the graphene-h-BN interface and possible polymer contamination from the graphene transfer process. After the illumination has been provided, the dip was still seen [Fig. 3(e)]. It has, however, changed its position to about -0.7 V. The change indicates that the electron doping level is higher within the graphene layer. This also proves that the illumination performed here has led to similar results to those reported for low-area illumination during RS measurements shown in Fig. 2.

The wide range mapping reveals more features not seen in the narrow range of bias voltage. The majority of the mapped surface has uniform levels of density of states, as seen in continuous imaging tunneling spectroscopy (CITS) maps in Figs. 3(b) and 3(c) which are shown at 1.5 and 2.5 V, respectively. There are, however, points where the higher value density of electron states can be seen. What is more, there are areas between each where the higher DOS overlaps for few bias voltages. Positions of those points show no correlation with the topography in Fig. 3(a), suggesting their structural origin. An exemplary dI/dV curve of such points is shown in Fig. 3(f). The most notable feature is three peaks seen at -3.3 V, 1.5 V, and 2.5 V, which we refer to as D1, D2, and D3, respectively. These lines are still seen after the illumination, as shown in Fig. 3(g). They are, however, shifted to -2.9 V, 2.1 V, and 3.1 V, respectively. The direction of the shift of those states during the illumination is opposite to that of the Dirac point. This suggests that while the electron doping of the graphene layers increased, the lines are related to the material, in which the electrons escape after the process. Taking this fact into the consideration and the fact that the increase in the electron concentration of graphene is related to the escape of the electrons from h-BN during the illumination of the graphene/h-BN heterostructures¹⁵ it can be assumed that the peaks are associated with the hexagonal boron nitride. Furthermore, prior to the illumination, the separation of the D1 and D3 peaks is estimated to be 5.8–6.0 eV. With this and recent reports revealing h-BN to have a wide indirect bandgap over 5.9 eV⁷ and the non-uniform distribution of those lines, it may be assumed that they are related directly to the conduction and valence bands or defect levels of the h-BN (Fig. 4). It is worth noting that unlike in the previously reported cases,³⁰ the potential of the tip does not seem to influence the charge state of the defect and the observed features are likely related to deep and, possibly, sub-surface defects. Considering that both D1 and D3 are close to the valence and conductivity bands, respectively, they may be related either to the Stone-Wales defects³¹ or nitrogen vacancies,³² while the D2 level may be associated with the boron vacancy, considering its located further away from both the bands.³² This, however, cannot be determined based on the STS curves alone. It is worth noting that the separation between D1, D2, and D3 levels changes after the illumination, as seen in Figs. 3(f) and 3(g). The value of the shift of

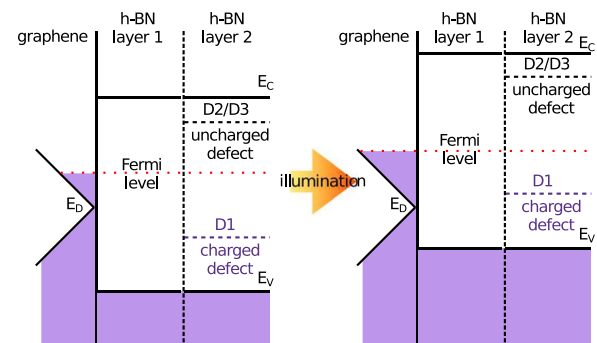


FIG. 4. Schematics of the shifting of bands and levels within graphene and h-BN during the illumination of the heterostructure. Illumination causes redistribution of the charge between different deep centers. This affects the position of the Fermi level in the structure.

D1 is similar to that of the Dirac point of graphene (0.35 eV–0.40 eV), suggesting that this change is related to the shifting of the quasi Fermi level. The shifts of D2 and D3 are higher. This behavior can be explained by the fact that the changes of the charge state of the defect centers involve shifting of the energy level within the bandgap. What is more, the phenomenon is related to the emergence of strain within the lattice.¹⁵

In summary, the behavior of MOVPE grown h-BN and graphene/h-BN heterostructures based on it has been investigated. The shown results prove that the previously reported mechanism of the laser-induced excitation of the deep defect centers in hexagonal boron nitride does occur in the studied cases. The STS measurements performed under the illumination confirmed that the process leads to the change of the Fermi level in both graphene and h-BN. This change is associated with changes in the charge state of the defects in h-BN, which lead to the emergence of local electric fields, which affects the graphene. The presented results prove the possibility of the study of the deep defect states in hexagonal boron nitride, which is important from the point of view of various applications, including single photon emitters. The phenomenon may also find application in non-invasive microstructure of planar van der Waals heterostructures of h-BN.

This work was supported by the National Science Centre project granted on the basis of the Decision No. DEC-2015/16/S/ST3/00451. The authors also acknowledge funding from the EU Graphene Flagship Core 2 (Grant Agreement No. 785219).

REFERENCES

- A. K. Geim and K. S. Novoselov, *Nat. Mater.* **6**, 183–191 (2007).
- C. Bai, Y. Yang, and X. Zhang, *Phys. E* **42**, 1431–1434 (2010).
- A. Y. Zhu, F. Yi, J. C. Reed, H. Zhu, and E. Cubukcu, *Nano Lett.* **14**, 5641–5649 (2014).
- X. Li, J. Shan, W. Zhang, S. Su, L. Yuwen, and L. Wang, *Small* **13**, 1602660 (2016).
- U. Chandni, K. Watanabe, T. Taniguchi, and J. P. Eisenstein, *Nano Lett.* **16**, 7982–7987 (2016).
- X. Li, S. Lin, X. Lin, Z. Xu, P. Wang, S. Zhang, H. Zhong, W. Xu, Z. Wu, and W. Fang, *Opt. Express* **24**, 134–145 (2016).
- G. Cassabois, P. Valvin, and B. Gil, *Nat. Photonics* **10**, 262–266 (2016).
- K. K. Kim, A. Hsu, X. Jia, S. M. Kim, Y. Shi, M. Hofmann, D. Nezich, J. F. Rodriguez-Nieva, M. Dresselhaus, T. Palacios, and J. Kong, *Nano Lett.* **12**, 161–166 (2012).

- ⁹C. R. Dean, A. F. Young, I. Meric, C. Lee, L. Wang, S. Sorgenfrei, K. Watanabe, T. Taniguchi, P. Kim, K. L. Shepard, and J. Hone, *Nat. Nanotechnol.* **5**, 722–726 (2010).
- ¹⁰X. Fan, R. Nouchi, and K. Tanigaki, *J. Phys. Chem. C* **115**, 12960–12964 (2011).
- ¹¹Q. Zhang, Y. Chen, C. Zhang, C.-R. Pan, M.-Y. Chou, C. Zeng, and C.-K. Shih, *Nat. Commun.* **7**, 13843 (2016).
- ¹²K. Cheng, Y. Guo, N. Han, X. Jiang, J. Zhang, R. Ahuja, Y. Su, and J. Zhao, *Appl. Phys. Lett.* **112**, 143902 (2018).
- ¹³Y. Chen, Y. Long, Y. Liu, L. Shen, Y. Zhang, Q. Deng, Z. Zheng, W. Yu, and S. Ruan, *Appl. Phys. Lett.* **103**, 063301 (2013).
- ¹⁴A. G. Kelly, D. Finn, A. Harvey, T. Hallam, and J. N. Coleman, *Appl. Phys. Lett.* **109**, 023107 (2016).
- ¹⁵I. Wlasny, R. Stepniewski, Z. Klusek, W. Strupinski, and A. Wyszomolka, *J. Appl. Phys.* **123**, 235103 (2018).
- ¹⁶C. Neumann, L. Rizzi, S. Reichardt, B. Terris, T. Khodkov, K. Watanabe, T. Taniguchi, B. Beschoten, and C. Stampfer, *ACS Appl. Mater. Interfaces* **8**, 9377–9383 (2016).
- ¹⁷G. Lupina, J. Kitzmann, I. Costina, M. Lukosius, C. Wenger, A. Wolff, S. Vaziri, M. Ostling, I. Pasternak, A. Krajewska, W. Strupinski, S. Kataria, A. Gahoi, M. C. Lemme, G. Ruhl, G. Zoth, O. Luxenhofer, and W. Mehr, *ACS Nano* **9**, 4776–4785 (2015).
- ¹⁸N. Petrone, C. R. Dean, I. Meric, A. M. van der Zande, P. Y. Huang, L. Wang, D. Muller, K. L. Shepard, and J. Hone, *Nano Lett.* **12**, 2751–2756 (2012).
- ¹⁹T. Uwanno, Y. Hattori, T. Taniguchi, K. Watanabe, and K. Nagashio, *2D Mater.* **2**, 041002 (2015).
- ²⁰B. Yates, M. J. Overy, and O. Pirgon, *Philos. Mag. A* **32**, 847–857 (1975).
- ²¹C. Handschin, P. Makk, P. Rickhaus, M.-H. Liu, K. Watanabe, T. Taniguchi, K. Richter, and C. Schenberger, *Nano Lett.* **17**, 328–333 (2017).
- ²²D. Chugh, J. Wong-Leung, L. Li, M. Lysevych, H. H. Tan, and C. Jagadish, *2D Mater.* **5**, 045018 (2018).
- ²³S. Reich, A. C. Ferrari, R. Arenal, A. Loiseau, I. Bello, and J. Robertson, *Phys. Rev. B* **71**, 205201 (2005).
- ²⁴M. Koperski, K. Nogajewski, and M. Potemski, *Opt. Commun.* **411**, 158–165 (2018).
- ²⁵R. V. Gorbachev, I. Riaz, R. R. Nair, R. Jalil, L. Britnell, B. D. Belle, E. W. Hill, K. S. Novoselov, K. Watanabe, T. Taniguchi, A. K. Geim, and P. Blake, *Small* **7**, 465–468 (2011).
- ²⁶A. Das, S. Pisana, B. Chakraborty, S. Piscanec, S. K. Saha, U. V. Waghmare, K. S. Novoselov, H. R. Krishnamurthy, A. K. Geim, A. C. Ferrari, and A. K. Sood, *Nat. Nanotechnol.* **3**, 210–215 (2008).
- ²⁷J. M. Urban, P. Dabrowski, J. Binder, M. Kopciuszyski, A. Wyszomolka, Z. Klusek, M. Jaochowski, W. Strupinski, and J. M. Baranowski, *J. Appl. Phys.* **115**, 233504 (2014).
- ²⁸A. H. Castro Neto, F. Guinea, N. M. R. Peres, K. S. Novoselov, and A. K. Geim, *Rev. Mod. Phys.* **81**, 109–162 (2009).
- ²⁹I. Wlasny, P. Dabrowski, M. Rogala, P. J. Kowalczyk, I. Pasternak, W. Strupinski, J. M. Baranowski, and Z. Klusek, *Appl. Phys. Lett.* **102**, 111601 (2013).
- ³⁰D. Wong, J. Velasco, Jr., L. Ju, J. Lee, S. Kahn, H.-Z. Tsai, C. Germany, T. Taniguchi, K. Watanabe, A. Zettl, F. Wan, and M. F. Crommie, *Nat. Nanotechnol.* **10**, 949–953 (2015).
- ³¹R. Wang, J. Yang, X. Wu, and S. Wang, *Nanoscale* **8**, 8210–8219 (2016).
- ³²B. Huang and H. Lee, *Phys. Rev. B* **86**, 245406 (2012).